

TRANSITION MECHANISMS IN LAMINAR SEPARATED FLOW UNDER SIMULATED LOW PRESSURE TURBINE AEROFOIL CONDITIONS

*Jerrit Dähnert

jerrit.daehnert@ilr.tu-berlin.de

*Christoph Lyko

christoph.lyko@ilr.tu-berlin.de

*Dieter Peitsch

dieter.peitsch@ilr.tu-berlin.de

*Institute for Aeronautics and Astronautics
Department of Aero Engines
Technical University of Berlin
Marchstraße 12-14, 10587 Berlin, Germany

ABSTRACT

Based on detailed experimental work conducted at a low speed test facility, this paper describes the transition process in the presence of a separation bubble with low Reynolds number, low free-stream turbulence, and steady main flow conditions. A pressure distribution has been created on a long flat plate by means of a contoured wall opposite of the plate, matching the suction side of a modern low-pressure turbine aerofoil. The main flow conditions for four Reynolds numbers, based on suction surface length and nominal exit velocity, were varied from 80,000 to 300,000, which covers the typical range of flight conditions. Velocity profiles and the overall flow field were acquired in the boundary layer at several streamwise locations using hot-wire anemometry. The data given is in the form of contours for velocity, turbulence intensity, and turbulent intermittency. The results highlight the effects of Reynolds number, the mechanisms of separation, transition, and reattachment, which feature laminar separation-long bubble and laminar separation-short bubble modes. For each Reynolds number, the onset of transition, the transition length, and the general characteristics of separated flow are determined. These findings are compared to the measurement results found in the literature. Furthermore, the experimental data is compared with two categories of correlation functions also given in the open literature: (1) correlations predicting the onset of transition and (2) correlations predicting the mode of separated flow transition. Moreover, it is shown that the type of instability involved corresponds to the inviscid Kelvin-Helmholtz instability mode at a dominant frequency that is in agreement with the typical ranges occurring in published studies of separated and free-shear layers.

INTRODUCTION

The focus in turbomachinery design is on weight reduction and increasing the efficiency of aerodynamic components. Weight reduction can be achieved by reducing the number of aerofoils in compressors and turbines through higher aerodynamic loading. Efficiency can be raised by improved control of the boundary layers on the bladings. This is particularly important for low pressure turbines of modern aircraft engines that develop high lift and operate at high-altitude flight conditions. Due to the small size of the blading, the elevated temperature level and the decreased density of air at altitude, Reynolds numbers are so low that large areas of the blade surface show laminar flow which is more prone to separation. Moreover the presence of separation can adversely affect the performance of these aerofoils, for which the laminar to turbulent transition plays an important role. An inaccurate analysis of the transition zone, the associated rates of aerodynamic loss production, and heat transfer can affect the efficiency by several per cent and the life of components significantly [17]. Therefore, the transition phenomena, especially in separated flows, have to be closely controlled.

Transition over a separation bubble is affected by many environmental factors [20], such as Reynolds number, pressure gradient, free-stream turbulence, surface roughness, noise, and vibration. In addition, turbomachinery flow is inherently unsteady in high quantities. It is common for the blades to shed wakes periodically. These wakes, in turn, travel downstream and periodically pass over the blades in the next row. Inside the wake is a region of elevated local freestream turbulence. HALSTEAD *et al.* [10] conclude the turbulence intensity can reach as high as 20%. The momentary high turbulence levels suppress bound-

ary layer separation although this effect is only temporary. The low turbulence intensity flow existing between shedding cycles is vulnerable to flow separation due to its laminar flow state [13]. This relationship could be a starting point of engineering design approach, by utilising these unsteady effects of blade row interaction.

However, little has been done so far to investigate the transition process with focus on the effects of periodic (velocity wake) and random (turbulence wake) components of the wakes. For most of the reported experiments, both phenomena are imposed simultaneously upon the boundary layer [9], [36] or have been introduced simultaneously while being controlled independently [19], [25]. Some attempts, however, have been made to investigate both effects separately [24], [16]. Both phenomena (velocity and turbulence wake) have a direct effect on the development of the boundary layer of the downstream blades.

To investigate the influences of these two phenomena on the transition process separately an experimental setup was designed which utilises the pressure distribution of the well known Pak-B blade profile. The present study was undertaken to provide a baseline data set for commissioning the new facility under steady low Reynolds number and conditions of low free-stream turbulence main flow. Complementary experimental work is underway covering the effect of main flow unsteadiness and elevated free-stream turbulence levels on transition mechanisms.

Numerous experimental studies have provided a great extent of knowledge regarding the parameters that affect transition involving separation bubbles under steady main flow conditions [14], [16], [22], [8], [33], [34], [35]. These investigations have been found to be particularly useful to the current study, by shedding light on the associated physical mechanism of the laminar-to-turbulent transition process under steady inflow conditions. Especially the research of LAKE *et al.* [13], MAHALLATI *et al.* [18] and VOLINO & HULTGREN [33] have been focused, since they all studied the Pak-B profile. The data published in [33] have been used to validate the experimental facility and to ensure the comparability of the results for further investigations.

Special attention was paid to the determination of separated flow transition modes and the type of instabilities which are involved in the transition process. In the absence of environmental disturbances, the laminar to turbulent transition of a separated shear layer is initiated by KELVIN-HELMHOLTZ (K-H) instability mode. According to DOVGAL *et al.* and MCAULIFFE [6], [21] the receptivity of the layer to small disturbances leads to a grouping of spanwise vorticities at selective streamwise wavelength, analogous to TOLLIEN-SCHLICHTING growth in attached boundary layers under low disturbance conditions. The growth of this separated shear layer instability results in a roll-up of the vorticity contained in the shear layer and leads to the growth of large-scale spanwise-oriented vortical structures, which interact with each other and provide the conditions under which a breakdown to small-scale turbulence and reattachment occurs. In contrast, in the presence of environmental disturbances, the formation and growth of turbulent spots in the separated shear layer can be observed [28], [9]. The length of

the transition region is determined by the merging and growth of these spots as they convect downstream, finally forming a turbulent shear layer during reattachment to the surface.

MCAULIFFE and YARAS [23] provide a comparative analysis of laminar-to-turbulent transition in separated shear layers, planar free shear layers, and boundary layers in environments of low disturbance. In all cases, the transition of the layer may primarily occur due to the inviscid K-H instability mode. In further work, MCAULIFFE and YARAS discussed the influence of the K-H instability mode on separated shear layers and the process of laminar-to-turbulent transition, similar to those observed on LP turbine blades. Both numerical and experimental investigations were carried out for a steady flat-plate boundary-layer flow with low Reynolds number that was developing in a streamwise pressure gradient. Experimentally, the pressure distribution was imposed by a contoured wall which formed the ceiling of the test section. MCAULIFFE [21] also provide a range of Strouhal numbers Sr_{2s} for shear flows, which have been correlated to transition due to K-H instability. A variety of studies concerning separated free- and boundary-layer shear flow are included and encompass the range $0.008 < Sr_{2s} < 0.016$ of Strouhal numbers.

HATMAN & WANG [11] considered cases on a flat plate under low free-stream turbulence conditions, various Reynolds numbers, and adverse pressure gradients. They distinguish three separated flow transition modes in their steady flow experiments. These were defined as a transitional separation mode, a laminar separation-short mode, and a laminar separation-long mode. For the laminar separation-short and -long mode, transition occurs downstream of the point of steady separation. They found that the dominance of one type of instability over the other (TOLLIEN-SCHLICHTING or KELVIN-HELMHOLTZ) determined the type of separation bubble.

Experiments have been carried out using a flat-plate boundary layer, which is subject to a streamwise pressure gradient corresponding to that on the suction side of the well-known "Pak-B" aerofoil. The focus of this paper is on the mean velocities and turbulence statistics, measured with a high temporal and spatial resolution at stations throughout the boundary layer. The effects of Reynolds number were determined and compared to the measurement results found in the literature. The results highlight the mechanism of separation, transition, and reattachment, which features laminar separation-long and -short bubble modes. In the present investigation, both modes of flow transition are shown to be induced downstream of the separation point by inflectional instability. For each mode, the onset of transition, the transition length, and the separated flow general characteristic are determined. Furthermore, the experimental data is compared with two categories of correlation functions also given in the open literature: (1) correlations predicting the onset of transition and (2) correlations predicting the mode of separated flow transition. Moreover, it is shown that the type of instability involved corresponds to the inviscid K-H instability mode at a dominant frequency that is in agreement with the typical ranges occurring in published studies of separated and free-shear layers.

EXPERIMENTAL SETUP

Experimental Facility

All experiments were conducted at the Technical University of Berlin in an unsteady low speed, open circuit wind tunnel of EIFFEL-type (Figure 1). The facility was used in earlier studies, such as LOU and HOURMOUZIADIS [16]. It incorporates an inlet, a settling chamber fitted with a honeycomb straightener and a series of screens, a square 9:1 contraction and a square test section of $0.4\text{ m} \times 0.4\text{ m} \times 1.5\text{ m}$ (width x height x length), shown in Figure 2. The test section is followed by a rotating flap and a diffuser. A blower placed downstream of the diffuser, with a variable-speed controller and which is capable of $2.5\text{ m}^3\text{s}^{-1}$, delivers air to the test section. The use of the rotating flap allows the creation of a periodic, unsteady inflow to the test section, by closing the passage twice each rotation [15] (not used in the present study).

For the present boundary-layer investigation, a flat plate of 1.0 m length is located in the test section (Figure 2). Particular attention was paid to surface finish, yielding excellent flatness ($\pm 5\text{ }\mu\text{m}/\text{m}$) and smoothness (average roughness $R_a = 0.5\text{ }\mu\text{m}$). The upper surface of this flat plate is the test wall for the experiments. A critical part in the design of the experiment was the leading-edge of the test plate. It is essential to avoid flow separation and instability since this would corrupt downstream measurements. Therefore a NACA0009-profile leading edge was chosen and preliminary measurements were conducted to ensure that the stagnation point is fixed on the upper surface at the leading edge for any Reynolds number considered here. A two-dimensional contoured wall opposite the test plate creates the desired pressure distribution, to match the suction side of the highly loaded "Pak-B" blade profile. This blade profile is an incompressible Mach-number scaled version of a conventional geometry used in commercial aircraft. The test section design was

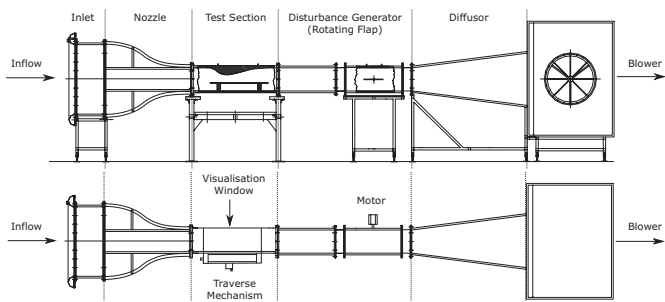


FIGURE 1. Periodic-unsteady low speed wind tunnel

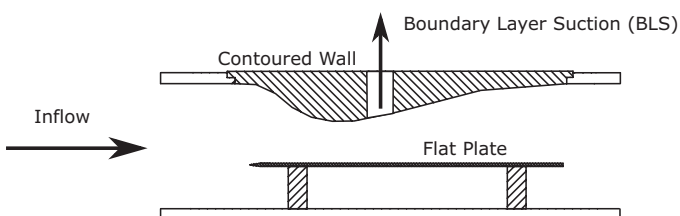


FIGURE 2. Test section

created by matching the mass flow from the generic LPT blade cascade through a flow channel with a contoured upper wall and a flat lower wall. An inviscid CFD method was used to compute the blade velocity and dimensionless pressure distribution. A wall was built opposite, with adjustable contours that were varied and tested until the pressure profile along the flat plate matched the dimensionless pressure distribution. To ensure that the flow only separated on the test surface and remains attached on the opposite wall, boundary-layer suction (BLS) was applied on the ceiling. It was placed just downstream the suction peak on a 40 mm streamwise segment with 260 holes covering the full span of the test section. The extent of boundary-layer suction was adjusted for each Reynolds number, to prevent separation as indicated by hot-wire boundary-layer traverses perpendicular to the contour. Furthermore, the opposite wall was covered by sandpaper both at the test section inlet and downstream from the BLS to ensure a turbulent boundary layer via tripping.

Instrumentation and data acquisition

At the back wall of the test section, a three-axis traversing mechanism holds the hot-wire probe, which can be set with an accuracy of 0.05 mm . The $5\text{ }\mu\text{m}$ diameter platinum single sensor hot-wire probe is operated together with a TSI IFA300 constant temperature anemometer (CTA) that measures the streamwise velocity. The hot-wire probe body was mounted at an angle of 30° relative to the test surface. Traversing was realised using stepper motors controlled by the same workstation used for data acquisition. The voltage signal had been conditioned using the TSI IFA300 and sampled using a 16-bit digitiser, which was controlled by a PCI bus interface. At each measurement point, 13s-long time records were obtained at a 10 kHz sampling rate

Station	1	2	3	4	5	6	7
x/L_{ss}	0.07	0.15	0.22	0.30	0.35	0.40	0.45
Station	8	9	10	11	12	13	14
x/L_{ss}	0.50	0.52	0.55	0.57	0.60	0.62	0.65
Station	15	16	17	18	19	20	21
x/L_{ss}	0.68	0.70	0.71	0.73	0.74	0.75	0.76
Station	22	23	24	25	26	27	28
x/L_{ss}	0.78	0.79	0.80	0.81	0.83	0.84	0.85
Station	29	30	31	32	33	34	35
x/L_{ss}	0.86	0.88	0.89	0.90	0.91	0.93	0.94
Station	36	37	38	39	40	41	42
x/L_{ss}	0.95	0.96	0.98	0.99	1.00	1.01	1.03
Station	43	44	45				
x/L_{ss}	1.04	1.05	1.06				

TABLE 1. Streamwise position of the measurement stations

using a hardware low-pass filter for anti-aliasing at 4 kHz before sampling. In order to ensure that enough was recorded, the square root of the integrated power spectral density curve (PSD curve) over the frequency domain at the location of maximum fluctuation velocity u'_{max} was compared to the rms value u' of the time record, with respect to the measurement uncertainty. The section of the test plate which represented the aerofoil covered $L_{ss} = 0.8$ m, while the actual plate was 1 m long. The last measurement station was downstream of the point representing the trailing edge of the aerofoil. Along the flat plate test surface, 45 velocity profiles were scanned at mid-channel width ranging from $x/L_{ss} = 0.07$ to 1.06 (Table1). Each profile consisted of 20 to 55 measurement positions, totalling 2,110 measurement points. To optimise the significance of these measurement points, 20 points per profile have been used for laminar unseparated flow and 55 points per profile for separated and reattaching flow, exponentially spaced perpendicular to the wall, with finer spacing closer to the surface. The estimated uncertainty of the measurement chain in mean and fluctuating velocities was determined to 5%, caused primarily by the bias error resulting from calibration. Using this relationship, the bias error can be cancelled by normalising the velocities on the free-stream velocity, leading to a level of uncertainty of 3% in the normalised quantities.

Calculation of derived quantities

To help interpret the transition process, several key parameters, such as the momentum thickness Reynolds number Re_2 , the shape factor H_{12} , the skin friction coefficient c_f , and the intermittency factor γ were computed from the measurement data. The following paragraphs describe the procedures that were used for calculating the mentioned quantities.

Skin friction coefficient c_f

For incompressible, fully developed turbulent as well as laminar flows with smooth solid walls, the non-dimensional mean velocity profile u^+ close to the wall may be written in the form

$$u^+ = f(z^+) \quad (1)$$

where

$$u^+ = \frac{u}{u_\tau}, \quad z^+ = \frac{z \cdot u_\tau}{\nu} \quad (2)$$

The function $f(z^+)$ in the viscous sublayer ($z^+ \leq 5$) is usually represented by

$$u^+ = z^+ \quad \text{for } z^+ \leq 5 \quad (3)$$

The wall shear velocity u_τ is estimated from experimental data using Eqn. (3), by the assumption of a linear velocity profile close to the wall. This method of estimating the wall shear stress,

which is referred to in literature as the *wall-slope method*, requires accurate velocity measurements in the near wall region.

Measurements with hot-wire sensors located very close to the wall are prone to additional error due to heat-transfer interaction between the probe sensor and the test surface. This fact emphasises that a minimum distance to the wall is needed in order to obtain reliable velocity information. A common method of sensor positioning was applied that employs a microscope to visually observe and measure the initial position of the sensor with respect to the wall.

To demonstrate that our measurements fulfil the needs for the extraction of skin friction information from the velocity gradients, Figure 3 shows existing data of DURST *et al.* and CHEW *et al.* for hot-wire readings close to heat-conducting walls compared to the present results and Equation (3). Figure

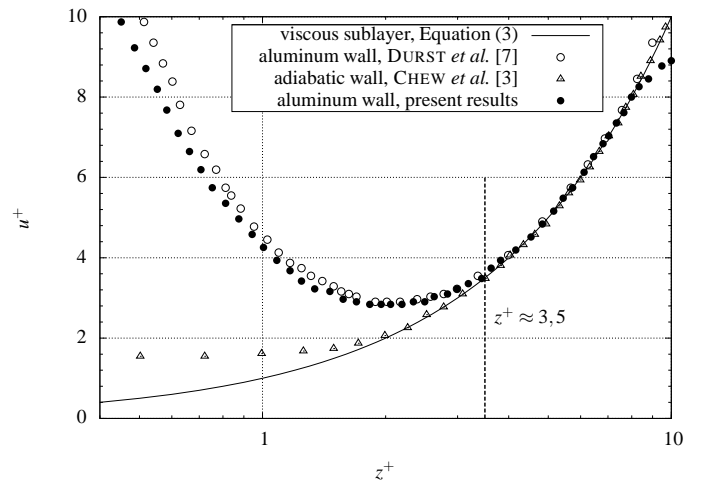


FIGURE 3. Near-wall effect on hot-wire readings, present results at $x/L_{ss} = 1.06$ for $Re_\infty = 300,000$

3 reveals that the hot-wire measurements are valid for all values of $y^+ \geq 3.5$. For the calculation of the skin friction coefficient a linear regression has been applied to a minimum of five velocity data points within the interval $3.5 \leq y^+ \leq 5.0$. This method's accuracy is estimate to be 8%. Within the separation bubble c_f was set to be zero, depending on a minimum threshold of this quantity. This assumption can be made here, since the measured mean velocities and the streamwise fluctuation velocities in the separation region are very close to zero, indicating that the extend of reverse flow in this area and thus c_f is also close to zero.

Displacement and momentum thickness δ_1, δ_2

The displacement thickness δ_1 and momentum thickness values δ_2

$$\delta_1 = \int_0^\infty \left(1 - \frac{u(z)}{U}\right) dz \quad (4)$$

$$\delta_2 = \int_0^\infty \frac{u(z)}{U} \left(1 - \frac{u(z)}{U}\right) dz \quad (5)$$

throughout the flow field were determined per Eqn. (4) and (5) using the time-averaged streamwise velocity profiles. Since the acquired data is discrete and not infinite, the integrals are solved numerically via quadrature substituting the upper integration limit by the upper border of the measurement window. The variation of the free-stream velocity is at the order of 0.5 % and thus the contribution of this region to both integrals is neglectable. Within the separation region this method can be applied with success, since the extend of reverse flow is very small as mentioned in the section on the skin friction coefficient.

Intermittency factor γ

The time traces of the digitised instantaneous streamwise velocity signal were analysed to compute the turbulent intermittency. The turbulent intermittency factor γ is defined as the time average of the intermittency function $\Gamma(t)$, which indicates whether the boundary layer is instantaneously turbulent or non-turbulent at a measurement location. $\Gamma(t)$ takes the value zero where flow is non-turbulent, and one where flow is turbulent. In the present study, the intermittency detection technique introduced by CHEW *et al.* [4] was utilised. It is based on the instantaneous streamwise velocity $u(t)$ from which time derivatives of the streamwise turbulent kinetic energy are obtained and compared to two threshold coefficients kept constant throughout the flow field. The threshold coefficients were adjusted according to the procedure described in CHEW *et al.* using various time traces of the instantaneous streamwise velocity $u(t)$ at characteristic locations throughout the flow field. From the large quantity of data, calculated results and the visual inspection of the instantaneous velocity signals, the determined coefficients can be satisfactorily taken in the transitional boundary layer. For convenience of detecting turbulent intermittency, a high-pass digital filter was applied to the streamwise velocity fluctuation $u'(t)$. The third-order BUTTERWORTH digital filter eliminates low-frequency fluctuations, which are common to both the turbulent and non-turbulent zones. It was chosen instead of a physical filter to preserve the original signal for further analysis.

Integral length scale

In order to provide the present data for validating CFD transition models, the longitudinal integral length scale Λ_x was evaluated from the power density spectrum of the streamwise velocity [2] for two free-stream locations, (1) the inlet and (2) the location of separation. The integral scales are representative of the large eddies in the free-stream. At the inlet and at the location of separation the longitudinal integral length scale and turbulence intensity were determined to $\Lambda_x = 6 \text{ mm}$, $Tu_x = 0.5\%$ and $\Lambda_x = 10 \text{ mm}$, $Tu_x = 0.4\%$ respectively. The integral scales did not vary notably with the Reynolds number.

RESULTS

Experimental results

The two-dimensional flow structure and the separation bubble formation were analysed for steady main flow conditions with

an inlet Tu_x of 0.5% at Reynolds numbers of 80,000, 100,000, 160,000 and 300,000. The data analysis was mainly focused on the major parameters, which determine the evolution of a separation bubble. All four experiments show similar characteristics. This paper describes in detail the flow structure of the $Re_\infty = 100,000$ and $Re_\infty = 300,000$ cases. The analysis and discussion will include results of the other cases to provide a complete understanding. Since, a better appreciation of the occurring transition modes is achieved with ascending pressure gradient parameter K_s , the four cases will be discussed in a descending order of Reynolds number.

Dimensionless streamwise pressure profiles for the four experiments are shown in Figure 4, along with the expected suction-side profile of the "Pak-B" aerofoil for high Reynolds number flow. The distribution of the pressure coefficient c_p , was computed utilising the boundary-layer edge velocity at the corresponding streamwise location. The streamwise coordinate is normalised on the nominal suction surface length. The main flow over the flat plate is first accelerated up to the velocity peak at $x_p/L_{ss} = 0.55$ and then diffused by the adverse pressure gradient. Upstream of the suction peak, the pressure coefficient is consistent with the expected suction side profile for all cases. Downstream, the c_p distribution diverges from the expected suction-side profile depending on the Reynolds number, which will be shown to arise due to the formation of a laminar separation bubble in all the cases considered. The larger the observed divergence, the bigger the extent of the separation zone. When $Re_\infty = 300,000$, this zone remains small, due to the high Reynolds number. With decreasing Reynolds number, the boundary layer is more prone to separation and the c_p values indicate a growth of the separation zone. The flow seems to reattach in the range $Re_\infty = 100,000$ to $Re_\infty = 300,000$. Since reattachment to the surface ensures the bubble's closing condition, it follows that the transition from laminar to turbulent must have taken place. At $Re_\infty = 80,000$, the boundary layer does not appear to reattach.

The momentum thickness Reynolds number Re_2 , the shape factor H_{12} , and the skin friction coefficient c_f are presented in Figure 5 for the measurement campaign. In all cases the shape factor H_{12} starts at the 1st station ($x/L_{ss} = 0.07$) with a laminar value of $H_{12} = 2.6$ (Figure 5b). As a result of the rapid acceleration of the boundary layer through the following stations, the shape factor decreases to $H_{12} \approx 1.9$ and remains near this level until the 10th station ($x/L_{ss} = 0.55$), which corresponds to the test section

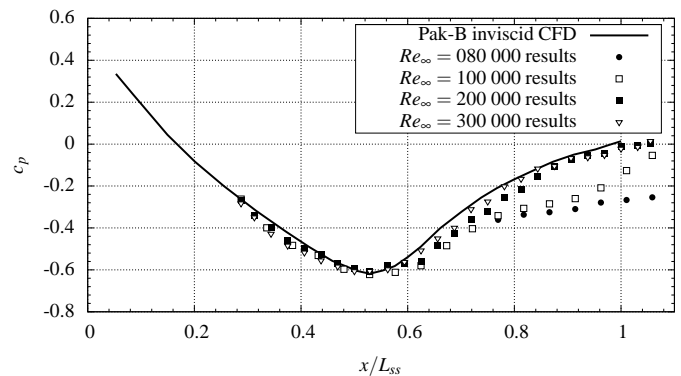


FIGURE 4. c_p distribution along the streamwise coordinate

throat area. This strong acceleration in the front portion of the flat plate is also evident in the skin-friction coefficient (Figure 5c). The tendency towards lower values of Re_2 in the interval $100 < Re_2 < 200$ compared to the laminar correlation for c_f is clearly notable. This can be explained by observing that this correlation is valid for zero pressure gradient cases only. In Figure 5a, the same region exhibits a very slow growth of Re_2 emphasizing the impact of the negative pressure gradient. Downstream of the throat, there is a step rise in $H_{12} = \delta_1/\delta_2$ for all cases, due to a rise in the displacement thickness δ_1 as the boundary layer separates. The maximum displacement of the boundary layer corresponds to the maximum of H_{12} indicating the onset of transition, which will be shown later. Downstream of the location of maximum displacement δ_1 the shape factor H_{12} decreases rapidly due to both a sharp rise in momentum thickness δ_2 and a strong decrease of the displacement thickness δ_1 . This behaviour is characteristic of transitional flow. Transition is identified by examining the intermittency distribution across the

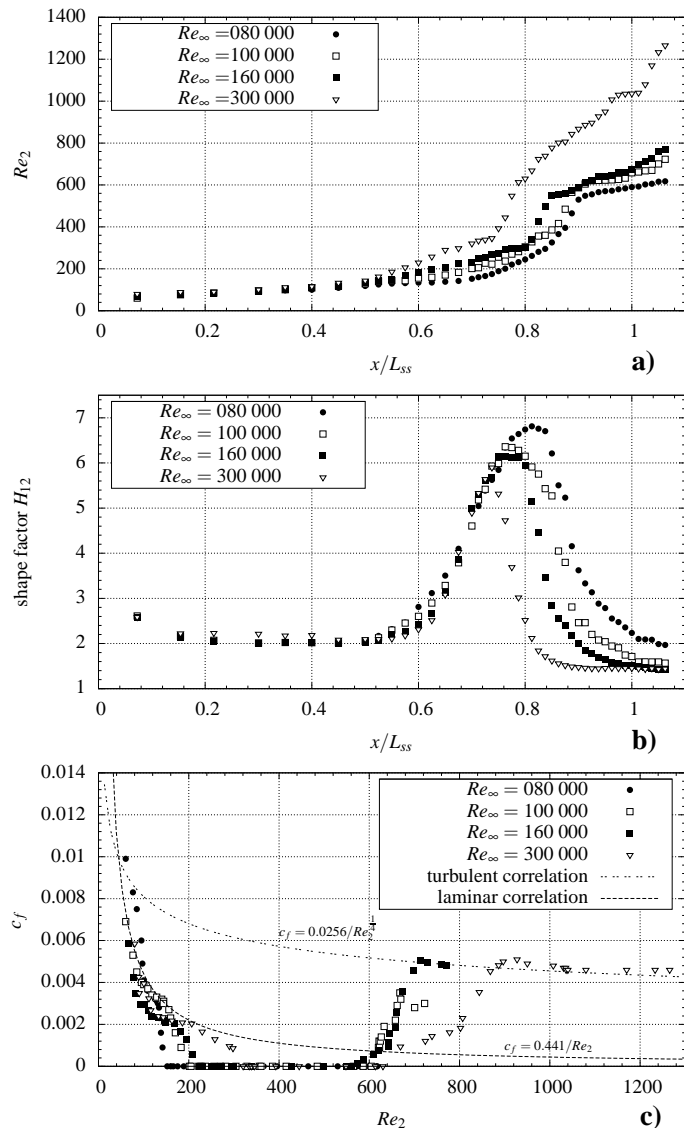


FIGURE 5. Momentum thickness Reynolds numbers (a); shape factor (b) and skin friction coefficient (c)

boundary-layer at the respective station.

The following sections explain the characteristics of transition at the various Reynolds numbers.

$Re_\infty = 300,000$ case

The mean streamwise velocity profiles, velocity field, and fluctuating velocity field, together with the intermittency field, are presented for all stations of the $Re_\infty = 300,000$ case in Figure 6. In order to gain a complete picture of the flow field, the acquired profile data has been (linearly) spatially interpolated. Mean velocity shows the expected laminar boundary layer profile for the first 10 stations, up to the throat. At station 15 ($x/L_{ss} = 0.68$), the velocity profile initially detaches from the wall, forming an inflection point near the wall, which shows that the separation point must be located within this station 15 ($x/L_{ss} = 0.68$) and the previous station 14 ($x/L_{ss} = 0.65$). Between stations 15 ($x/L_{ss} = 0.68$) and 19 ($x/L_{ss} = 0.74$), the boundary layer is clearly

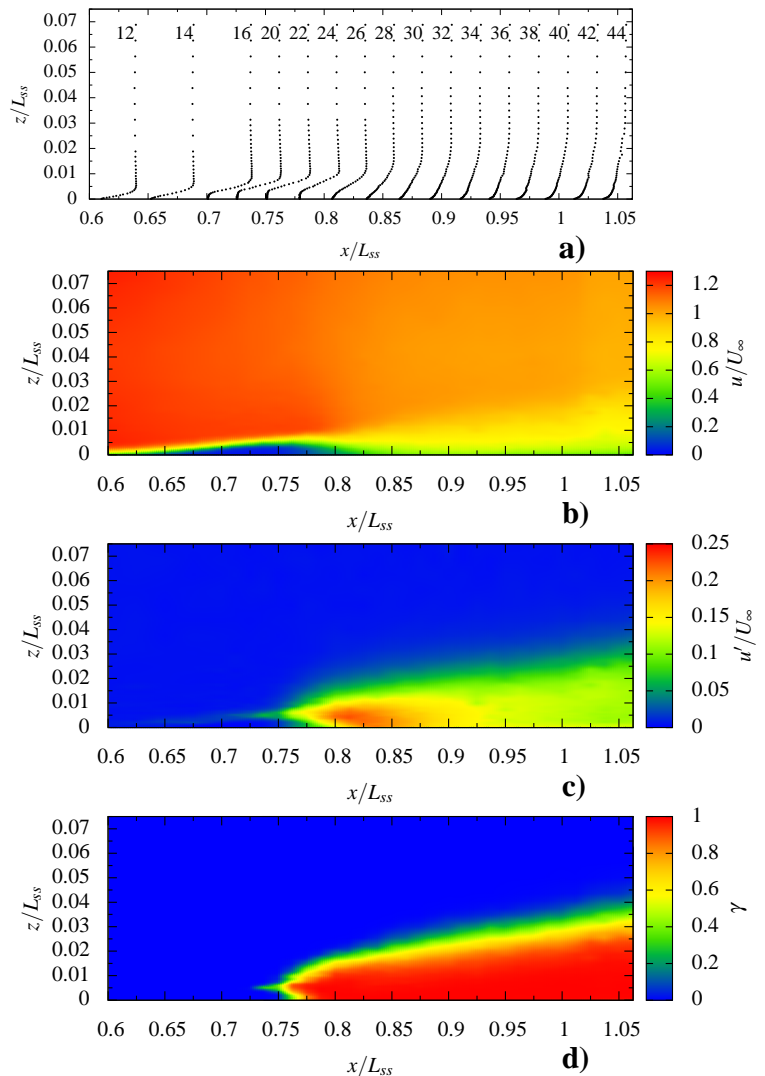


FIGURE 6. $Re_\infty = 300,000$ case: time-averaged velocity profiles* (a); time-averaged velocity field (b); fluctuation velocity field (c); intermittency field (d)

*subfigure a): qualitative representation of velocity profiles during stations 12 to 44; only every second profile shown

separated and the separation bubble is growing. At station 19 ($x/L_{ss} = 0.74$), the maximum bubble elevation corresponding to $H_{12,max}$ is reached. Also this location is where the first occurrence of non-zero values of the intermittency factor are seen, indicating the onset of transition. Spectral analysis comes next, disclosing a broad band frequency peak, which grows during the very next downstream stations. As the very first case, the $Re_\infty = 300,000$ case returns to lower H_{12} , indicating ongoing transition of the boundary layer. At station 25 ($x/L_{ss} = 0.81$), the low, but non-zero velocity near the wall indicates that the boundary layer is reattaching and the separation bubble is closed. It is interesting to note that this observation fits with the maximum fluctuation velocity u'_{max} for the same station. This fact gives a hint regarding the separational transition mode, as documented by HATMAN & WANG [11]. According to their investigations and published correlations, the separation bubble at $Re_\infty = 300,000$ can be identified as one in short mode. The boundary layer further diffuses under the adverse pressure gradient and achieves the fully turbulent state by the 26th station ($x/L_{ss} = 0.83$), as indicated by the intermittency factor γ approaching to unity throughout the profile at this station. These observations of separation, transition, and reattachment are also consistent with the distribution of the skin friction coefficient shown in Figure 5c.

$Re_\infty = 100,000$ case

The same quantities are presented in Figure 7 for the $Re_\infty = 100,000$ case. Up to the suction peak, all available data shows almost the same behaviour of the boundary layer as described above. The first detached velocity profile can be observed at station 14 ($x/L_{ss} = 0.65$), followed by a step rise in H_{12} and an increase of Re_2 that suggests separation to take place. Compared to the $Re_\infty = 300,000$ measurements, separation occurs one station earlier. Thus the point of separation seems to vary only marginally as a function of Reynolds number, which is consistent with the other cases considered. At station 25 ($x/L_{ss} = 0.81$), the maximum bubble elevation corresponding to $H_{12,max}$ is achieved. In contrast to the $Re_\infty = 300,000$ case described above, a plateau forms in the shape factor distribution around $H_{12,max}$. In the region of this plateau, the fluctuation velocities (Figure 7c) exhibit a rise in amplitude which remains spatially limited over a few measurement points. An evaluation of the frequency spectra confirm the onset of transition by the presence of a periodic disturbances of small amplitude. The frequency of this phenomena can be linked to the inviscid K-H instability, as the oscillation scales with the range of separation Strouhal numbers Sr_{2s} , which is typical for these shear-layer instabilities. With the end of the plateau at station 25 ($x/L_{ss} = 0.81$), H_{12} starts to decrease, indicating the onset of transition. At the following stations 26 ($x/L_{ss} = 0.83$) to 33 ($x/L_{ss} = 0.91$), a rise in amplitude of the streamwise fluctuation velocity u' together with a sudden flare-up in γ can be observed. The intermittency factor γ then rapidly spreads out and the transition process leads to a first "weak" reattachment (at x_{R1}) as the low, but non-zero velocity near the wall suggests. At station 34 ($x/L_{ss} = 0.93$), the maximum fluctuation velocity u'_{max} is achieved. At the following stations 35 ($x/L_{ss} = 0.94$) to 45 ($x/L_{ss} = 1.06$), the rate

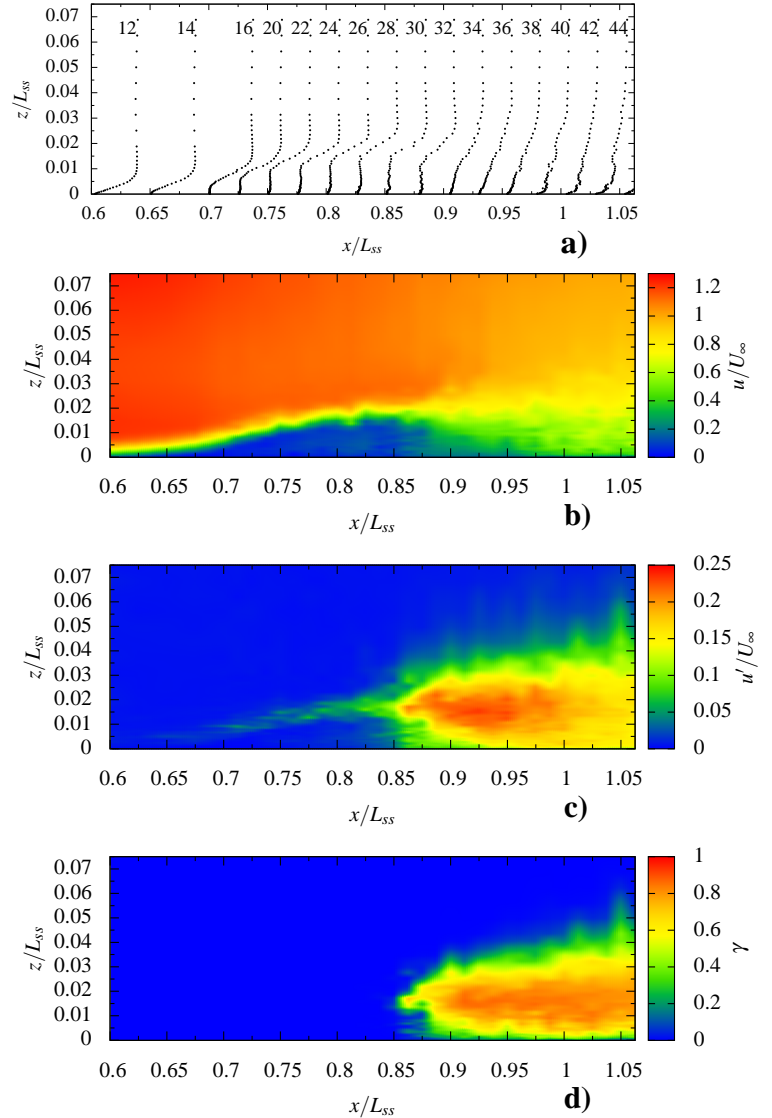


FIGURE 7. $Re_\infty = 100,000$ case: time-averaged velocity profiles* (a); time-averaged velocity field (b); fluctuation velocity field (c); intermittency field d)

* subfigure a): qualitative representation of velocity profiles during stations 12 to 44; only every second profile shown

of decrease in H_{12} reduces notably (Figure 5b) and can be construed as being a sign of transition delay. Since the "weak" reattachment led to a reduction of bubble elevation but incomplete reattachment, the mixing is reduced and the transition completion is delayed. Finally, at stations 38 ($x/L_{ss} = 0.98$) through 45 ($x/L_{ss} = 1.06$), the coalescence into turbulence forces the "final" reattachment at x_R (station 38 ($x/L_{ss} = 0.98$)) and a closed long bubble results. These facts are in accordance with the mechanisms described by HATMAN & WANG [11]. All but one criteria matched the proposed laminar separation-long bubble mode for the $Re_\infty = 100,000$ case. The criterion not accomplished regards the end of transition, matching the location of "final" reattachment. At this station and further downstream, the intermittency factor γ indicates a maximum value of $\gamma = 0.65$, which implies that in this case, the flow still remains transitional after reattachment. Again, these observations are also consistent with the distribution of the

skin friction coefficient shown in Figure 5c. The skin friction coefficient that corresponds to the very downstream station, with a maximum value of Re_2 , lies between the two correlation functions clarifying transitional flow.

$Re_\infty = 160,000$ & $Re_\infty = 80,000$ cases

Up to the suction peak, data of the $Re = 80,000$ and $Re_\infty = 160,000$ case shows almost the same of the boundary-layer behaviour. Both cases can be identified as being of laminar separation-long bubble mode comparable to the $Re_\infty = 100,000$ case. However, some differences can be observed compared to the cases described above.

At $Re_\infty = 160,000$ the start of transition, and its completion occurs earlier compared to the $Re_\infty = 100,000$ case, which is evident in the sudden rise of Re_{2s} shown in Figure 5a, indicating transition. The faster transition completion can be concluded from the shape factor H_{12} (Figure 5b), which reaches lower value of H_{12} before the last measurement station in comparison to the $Re_\infty = 100,000$ case. The skin friction coefficient (Figure 5c) is once again in accordance with these observations. The reasons for this boundary-layer behaviour is connected to the higher Reynolds number. The effects of increasing the Reynolds number are twofold: (1) the shear layer instability grows to a larger maximum amplitude and (2) the rate of growth is increased. Both effects lead to an earlier transition onset and faster completion of the process.

In case of the $Re_\infty = 80,000$ measurements, the visual inspection of the velocity profiles indicates a still detached shear layer, as previously assumed from the pressure distribution (Figure 4). However, the onset of transition is present and the mixing in the region of maximum u'_{max} as well as the high rate of momentum transport inward and toward the wall lead to a reduction of bubble elevation. Thus the mixing is reduced, the transition process is delayed, and the shear layer fails to reattach to the surface. With the last measurement station, the shape factor reaches a value of $H_{12} = 1.98$ (Figure 5b), while the distribution of the skin friction coefficient (Figure 5c) gives evidence for the transitional state of the boundary layer.

Transition and separation locations

The locations of separation x_s , transition start x_t , first reattachment x_{R1} , maximum fluctuation velocity $x_{u'_{max}}$, final reattachment x_R , transition end x_T , and the conditions at the separation point in terms of Sr_{2s} , Re_{2s} , H_{12s} , K_s and Po_s are summarised in Table 2.

The separation locations are determined by visual inspection of the velocity profiles, aided by an evaluation of the skin friction coefficient c_f . It is the high spatial resolution of measurement stations in streamwise direction, allowing this simple technique to give an accuracy of 1.25% without the need for data extrapolation. From Table 2, we see that the main parameters describing the separation bubble listed, i.e., the shape of the separation bubble, the separation point, and the resulting length of transition, all obviously depend on two factors: the Reynolds number and the actual pressure distribution, which is influenced by the

Re_∞	80,000	100,000	160,000	300,000
x_s/L_{ss}	0.65	0.65	0.68	0.68
x_t/L_{ss}	0.83	0.81	0.80	0.75
x_{R1}/L_{ss}	-	0.93	0.86	-
$x_{u'_{max}}/L_{ss}$	0.95	0.93	0.86	0.81
x_R/L_{ss}	-	0.98	0.93	0.81
x_T/L_{ss}	-	-	1.03	0.83
Sr_{2s}	0.014	0.011	0.009	0.009
Re_{2s}	138	168	211	295
H_{12s}	2.81	3.29	3.12	3.50
$K_s \times 10^{-6}$	-4.2	-3.05	-1.93	-0.919
Po_s	-0.084	-0.085	-0.086	-0.080

TABLE 2. Parameters describing the separation bubble in the four test cases

separation itself. The most suitable non-dimensional parameter describing this pressure distribution in the region of the bubble is the acceleration parameter, given by $K = (v/U^2) (dU/dx)$. This parameter varies between $-4.2 \cdot 10^{-6}$ and $-0.919 \cdot 10^{-6}$ for the four test cases. The POHLHAUSEN parameter at the separation point, given by $Po_s = Re_{2s}^2 K_s$, is between -0.080 and -0.086 over the Reynolds number range investigated and correlates the empirical value -0.082 suggested by THWAITES [31]. While the point of separation changes marginally with the Reynolds number, the start of transition varies significantly. The differences in transition length can be explained by changes in transition mode.

HATMAN & WANG developed a prediction model for distinguishing three separated-flow transition modes: transitional separation, laminar separation-short bubble and laminar separation-

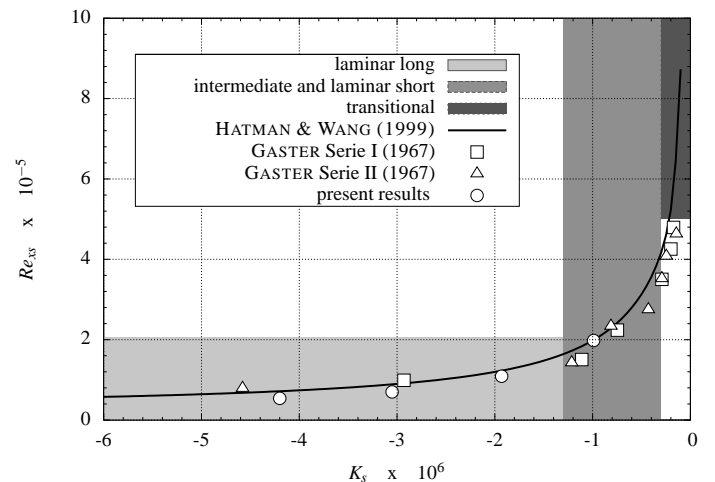


FIGURE 8. Correlation between separation Reynolds number and pressure gradient parameter at separation: $Re_{xs} = f(K_s)$

long bubble [11]. The first mode involves transition starting upstream of the separation point, with the latter two having the onset of the transition downstream of the separation point by inflectional instability. The separated flow transition in the current study can be identified as laminar separation-short bubble for the case of $Re_\infty = 300,000$ and laminar separation-long bubble for the other Reynolds numbers cases, as shown with results in Figure 8. Furthermore transition is observed to occur abruptly in the $Re_\infty = 300,000$ case, emphasised by the rapid spreading of intermittency shown in Figure 6d. In contrast the lower Reynolds number cases exhibit a transition delay as discussed in the previous sections. These results are in accordance with the correlations of HATMAN & WANG and MAYLE [20] and clarify, that short bubbles have only a small (local) downstream effect on the external potential flow whereas long bubbles can effect the pressure distribution upstream and downstream (global) of the separation location.

Instability characteristics

As mentioned in the introduction, MCAULIFFE and YARAS [23] provide a range of Strouhal numbers Sr_{2s} for shear flows, which have been correlated to transition due to K-H instability. This relationship is of particular relevance for all the cases investigated here. To aid the analysis of the separated shear layer transition process, turbulent power spectra at streamwise measurement locations from the suction peak to the trailing edge have been inspected. At each streamwise location, spectra were acquired with a single-sensor hot-wire probe at the wall-normal coordinate where the maximum fluctuating streamwise velocity u'_{max} was observed. For the four Reynolds numbers 80,000, 100,000, 160,000, and 300,000, the spectra indicate a peak frequency at the measurement station just downstream of the laminar separated shear-layer extent. Figure 9 exemplarily shows the frequency behaviour by the spectra obtained for the $Re_\infty = 300,000$ case.

All downstream measurement stations show a broadband

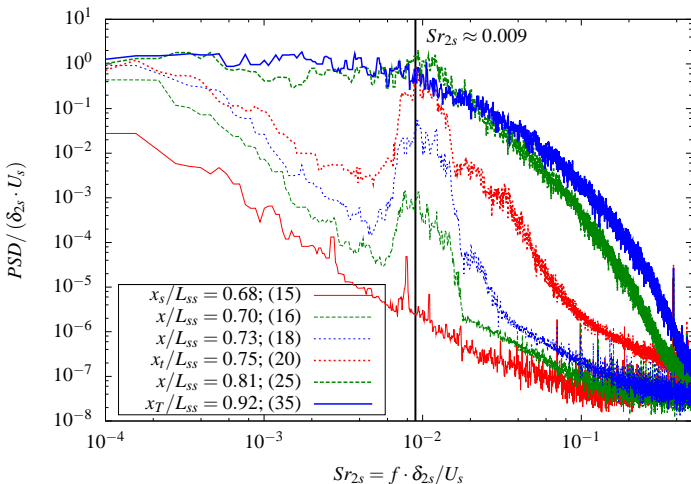


FIGURE 9. $Re_\infty = 300,000$ case: power spectra of streamwise velocity at six stations within the separated shear layer

rise in power over the higher frequency range, suggesting the observed peak to correspond with the free shear layer instability, which initiates transition of the shear layer to turbulence. For the investigated cases, the momentum thickness Strouhal number calculated at the separation point, is between $0.009 < Sr_{2s} < 0.014$, with a trend to lower values for higher Reynolds numbers. In all cases, transition occurs through the amplification of disturbances via an inviscid K-H instability mode at a dominant frequency that is in agreement with the typical ranges occurring in published studies of separated and free shear layers. This confirms the K-H instability mode correlations summarised by MCAULIFFE [21].

Investigators	$Sr_{2s} = f \cdot \delta_{2s} / U_s$
present study	0.009-0.014
TALAN & HOURMOUZADIS [30]	0.010-0.014
MCAULIFFE & YARAS [22], [23]	0.008-0.016
PAULEY <i>et al.</i> [27], [14]	0.005-0.008
YANG & VOKE [32]	0.005-0.011
HO & HUERRE [12] <small>(free-shear layer Sr_2)</small>	0.016

TABLE 3. Instability Strouhal numbers identified in several studies involving shear layers with inflectional velocity profiles

Table 3 shows the present experiments and a variety of studies concerning separated free- and boundary-layer shear flow which encompass the range $0.008 < Sr_{2s} < 0.016$ of Strouhal numbers.

Comparison to correlations

Several correlations for predicting the location of transition onset for separated flow transition are given in the literature. On the basis of the present measurement results, a comparison between some of these correlations is given below.

MAYLE [20] presents two correlations for the starting location that account for the transition process within the free shear layer, resulting in short or long separation bubbles. Here, the terms "long" and "short" are in accordance with the nomenclature of HATMAN & WANG [11].

$$(Re_x)_{st} = Re_{xt} - Re_{xs} = 1000 \cdot Re_{2s}^{0.7} \quad \text{long bubble} \quad (6)$$

$$(Re_x)_{st} = Re_{xt} - Re_{xs} = 300 \cdot Re_{2s}^{0.7} \quad \text{short bubble} \quad (7)$$

Figure 10 compares the results of the current study, to the above cited correlations given by MAYLE [20]. The Reynolds number based on the free-stream velocity at separation and the distance from separation to transition start $(Re_x)_{st} = Re_{xt} - Re_{xs}$ are plotted against the momentum thickness Reynolds number at separation Re_{2s} . In addition, measurement results of GASTER [8] and BELLOWS [1] are shown, which are the basis of the correlations given in Equations 6 and 7.

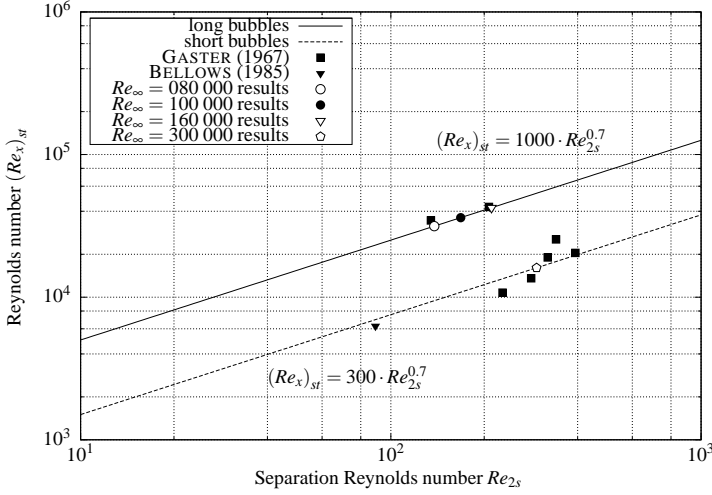


FIGURE 10. Distance between separation and transition as a function of the momentum thickness Reynolds number at separation

At first sight, the present results in all the four test cases considered suggest an excellent agreement with the correlations given by MAYLE [20], due to the reduced resolution of a double-logarithmic scale. In fact, the agreement of all long bubble cases is rather poor as shown later in Figure 11. However, a classification of separation bubble type and thus transition mode can be made similar to HATMAN & WANG [11], Figure 8.

HATMAN & WANG also provide a correlation in terms of $(Re_x)_{st}$ as

$$(Re_x)_{st} = 0.0816 Re_{xs} + 26805. \quad (8)$$

Further correlations for the onset of transition taking into account multiple parameters are given by DAVIS *et al.* [5], and YARAS [35], PRAISNER & CLARK [26], and VOLINO & BOHL [34].

DAVIS *et al.* [5] modified a model involving separation bubbles developed by ROBERTS [29], utilizing the free-stream turbulence level

$$(Re_x)_{st} = 25000 \log_{10} [\coth(0.1732 Tu)]. \quad (9)$$

YARAS [35] formulates

$$(Re_x)_{st} = 0.04 Re_{xs} + 6.3 \cdot 10^4 [1 - \tanh^3(TF')], \quad (10)$$

where $TF' = \max(TF, 1\%)$, and $TF = Tu(x_s/\Lambda)^{0.2}$. Herein Λ is the integral length scale of the free-stream turbulence and x_s is the distance from the leading edge to the separation point.

PRAISNER & CLARK [26] present the following correlation based on the momentum thickness Reynolds number at separation

$$(Re_x)_{st} = 173 Re_s Re_{2s}^{-1.227}. \quad (11)$$

VOLINO & BOHL [34] account for the fact that boundary-layer instabilities start to grow with the beginning of the adverse pressure gradient region, presenting the following correlation

$$Re_{pt} = 8.80 = [6.37 - \log_{10}(Tu^2)] Re_{2p}^{4/3}. \quad (12)$$

In this correlation, Re_{pt} is based on both the distance from the suction peak to the transition start and the free-stream velocity at the suction peak, while Re_{2p} represents the momentum thickness Reynolds number at this point.

The correlations summarised in Equations (6) to (12) were used to calculate x_t , which is defined as the distance from the leading edge to the start of transition. For Equations (9), (10), and (12), Tu was set to 0.5% according to the measured inlet turbulence intensity. The locations of separation x_s and suction peak x_p , together with the momentum thickness corresponding to these positions Re_{2s} and Re_{2p} , were taken from the experimental data. The resulting x_t are plotted in a non-dimensional form against the Reynolds numbers used with the correlations. The transition locations, as determined from the experimental data, are also shown. In case of data points where $x_t/L_{ss} > 1$, transition is predicted downstream of the trailing edge of the aerofoil.

Figure 11 compares the results of the current study, to correlations given by the above cited authors. One general observation may be made regarding the spread of transition onset within the correlation results: with decreasing Reynolds number the correlation results cover a wider range of possible transition onsets. Three of the considered correlations (Equations 6, 8, and 11) clearly tend to over predict the onset of transition for all Reynolds numbers investigated. The long bubble correlation of MAYLE [20], which is only intended for separation bubbles that reattach, was the correlation that over predicted the transition onset the most. In contrast, the formulation for the short bubble correlation is only slightly under predicted for the $Re_{\infty} = 300,000$ case. The two correlations given by VOLINO & BOHL [34] and DAVIS *et al.* [5] exhibit excellent agreement with the experimen-

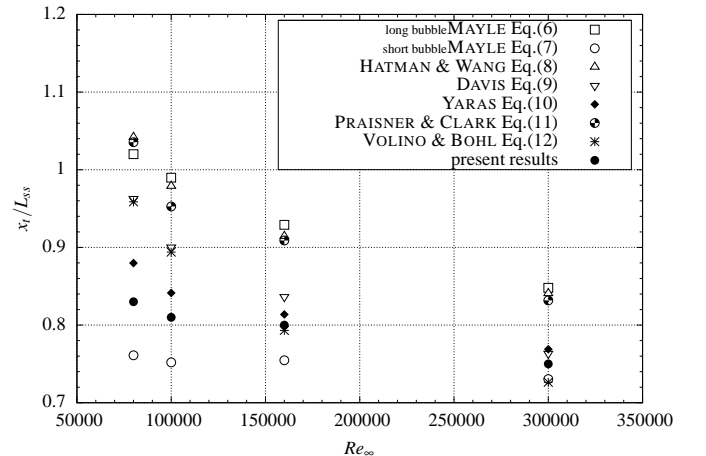


FIGURE 11. Location of transition onset as a function of the Reynolds number

tal results for the two highest Reynolds number cases. For the lower Reynolds numbers, both functions tend to predict transition onset too far downstream. For all Reynolds number cases, the YARAS [35] correlation agrees excellently with the present measurement results, showing a maximum deviation of 5% and a slight tendency towards higher values. Looking at these results, it can be concluded, that the best approximation of transition onset is given by the models that explicitly include the effects governing transition: (1) Reynolds number and (2) turbulence level. These correlations are formulated by YARAS [35] and VOLINO & BOHL [34].

Comparison to similar experimental investigations

The results presented in the previous sections are very similar to those resulting from a study of VOLINO & HULTGREN [33]. In this work, the boundary layer in a low-speed wind tunnel was subject to the same non-dimensional pressure distribution imposed on a flat plate by an opposite contoured wall. The range of Reynolds numbers ($Re_\infty = 50,000$ to $300,000$) considered by these authors is comparable to the present study, covering cruise to take-off conditions of an LP-Turbine. In both experimental efforts, transition in the low turbulence level cases occurs abruptly, leading to reattachment, while a strong dependence of transitional behaviour on the Reynolds number is noted. Since for two Reynolds numbers a direct comparison is possible, Figure 12 shows an example comparison of the pressure distribution for the Reynolds numbers $Re_\infty = 100,000$ and $300,000$ between both experiments. For each measurement point, the calculated

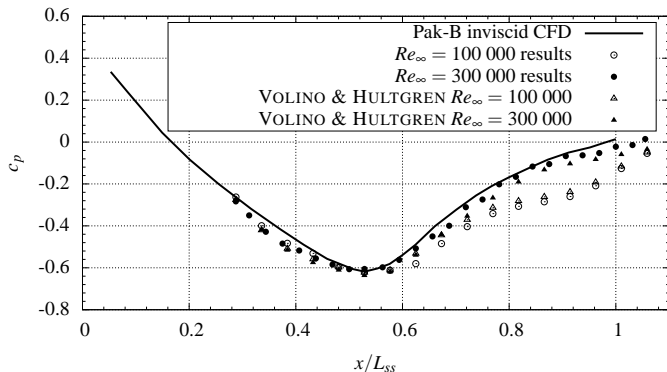


FIGURE 12. c_p distribution along the streamwise coordinate

difference of c_p between both studies lies within the approximated measurement uncertainty. In addition to the present investigation, VOLINO & HULTGREN [33] (2001) accounted for low and high free-stream turbulence levels with $Tu = 0.2\%$ and $Tu = 2.5\%$ respectively. An examination of the velocity profiles, the fluctuation velocity profiles, and the intermittency profiles reveals similarity between the results of the studies. However, beside strong similarities, some small differences in the location of transition onset and reattachment can be observed.

The separation location in the comparison of the experimental investigations exhibits a small difference of $\Delta x_s/L_{ss} = 0.01$. For both Reynolds number cases, the boundary-layer separates

by this distance further upstream in the present study. The onset of transition in the $Re_\infty = 100,000$ case can be determined about $\Delta x_t/L_{ss} = 0.07$ earlier, compared to the results of VOLINO & HULTGREN.

These differences may be due to slight deviations of the actual streamwise pressure gradients in the two experimental efforts, even though nominally the same. Since separation occurs at slightly different locations, it might have slightly altered the local pressure distribution between both studies, leading to different locations of transition onset. In case of the $Re_\infty = 300,000$ measurements, only a marginally difference of earlier transition onset ($\Delta x_t/L_{ss} = 0.01$) can be found. Analogues to the present results for the two Reynolds numbers, earlier reattachment is evident and can be quantified in $\Delta x_R/L_{ss} = 0.04$ and $\Delta x_R/L_{ss} = 0.01$ for the $Re_\infty = 100,000$ case and the $Re_\infty = 300,000$ respectively. It should be noted that in case of the $Re_\infty = 100,000$ results, the point of the first "weak" reattachment x_{R1}/L_{ss} is in agreement with the results of VOLINO & HULTGREN. The authors performed their experiments with a smaller number of overall measurement stations, resulting in a lower spatial resolution. So it seems that in their experiments, they could not resolve the final reattachment.

Nevertheless, the agreement of the measurement results between both studies cover most of the locations of transition characteristics within $\Delta x/L_{ss} = 0.01$. In the present work, separational transition modes according to HATMAN & WANG [11] could be identified, and the shear-layer instability being of inviscid K-H type could be recognised.

CONCLUSION

The following conclusions may be drawn from the present experimental results:

- Under low free-stream turbulence and Reynolds number conditions, transition is initiated through receptivity of the laminar separated shear layer to small disturbances and is dominated by the shear-layer instability.
- The frequency of the shear layer instability is found to be consistent with the inviscid KELVIN-HELMHOLTZ instability for all considered cases.
- Higher Reynolds numbers result in earlier transition within the separated shear layer and a reduced spatial extent of the separation zone (bubble length)
- The present study confirms the results of earlier workers, who suggested that transition at low turbulence levels is initiated within the separated shear layer due to the instability waves.
- The comparison of these results with correlations found in the literature suggests that the best approximation of transition onset is given by the model that explicitly includes the effects of (1) Reynolds number and (2) turbulence level.
- The newly built-up test rig delivered reliable and consistent data and can be used for further investigations regarding the effect of periodic unsteady free stream.

ACKNOWLEDGMENT

The authors gratefully acknowledge the support by Thomas Praisner of Pratt & Whitney for providing the "Pak-B" Geometry. In addition the authors would also like to thank Prof. Ralph J. Volino of the U.S. Naval Academy for supplying us with his measurement results as a comparative basis for this work. Finally, the authors are pleased to thank Alexander Heinrich for his advice and assistance in the final preparation of this paper.

NOMENCLATURE

c_f	skin friction coefficient, $2\tau_{wall}/(\rho U^2)$
c_p	pressure coefficient, $c_p = 1 - (U/U_\infty)^2$
f	frequency
K	pressure gradient parameter, $K = (v/U^2)(dU/dx)$
H_{12}	boundary-layer shape factor, $H_{12} = \delta_1/\delta_2$
L_{ss}	nominal suction surface length, $L_{ss} = 0.8 m$
Po	POHLHAUSEN parameter
R_a	average surface roughness (ISO 4287-1997)
Re	Reynolds number
Sr	Strouhal number
Tu	free-stream turbulence intensity
t	time
U	local free-stream velocity
u	local streamwise velocity
u'	rms fluctuating streamwise velocity
u^+	non-dimensional mean velocity, $u^+ = u/u_\tau$
u_τ	wall shear velocity, $\sqrt{\tau_{wall}/\rho}$
x, y, z	Cartesian coordinates
x	Cartesian coordinate in streamwise direction
z	Cartesian coordinate perpendicular to the test surface
z^+	non-dimensional wall distance, $z^+ = \frac{z u_\tau}{\nu}$
δ_1	displacement thickness
δ_2	momentum thickness
Γ	intermittency function
γ	intermittency factor
Λ	integral length scale
ρ	fluid density
ν	kinematic viscosity
τ_{wall}	wall shear stress in main flow direction

Subscripts

1	based on δ_1 and local free-stream Velocity
2	based on δ_2 and local free-stream Velocity
max	maximum value
R	final reattachment
$R1$	first reattachment
p	suction peak
s	separation
T	end of transition
t	beginning of transition
u'_{max}	value at maximum streamwise fluctuation velocity
x	based on surface coordinate in streamwise direction
∞	nominal exit value at $x/L_{ss} = 1$; based on nominal exit values

REFERENCES

- [1] Bellows, W. J., 1985. "An experimental study in leading edge separating-reattaching boundary layer flows". PhD thesis, Rensselaer Polytechnic Inst., Troy, NY.
- [2] Cebeci, T., and Smith, Apollo Milton Olin, ., 1974. *Analysis of turbulent boundary layers / Tuncer Cebeci and A.M.O. Smith*. Academic Press, New York :.
- [3] Chew, Y., Khoo, B., Lim, C., and Teo, C., 1998. "Dynamic response of a hot-wire anemometer. part ii: A flush-mounted hot-wire and hot-film probes for wall shear stress measurements". *Measurement Science and Technology*, **9**, May, pp. 764–778.
- [4] Chew, Y. T., Shah, D. A., and Wan, J., 1999. "An envelope method for detection of turbulence intermittency in a transitional boundary layer". *Fluid Dynamics Research*, **24**, pp. 7–22.
- [5] Davis, R., Carter, J. E., and Reshotko, E., 1987. "Analysis of transitional separation bubbles on infinite swept wings". *AIAA Journal*, **25**, pp. 421–428.
- [6] Dovgal, A., Kozlov, V., and Michalke, A., 1994. "Laminar boundary layer separation: Instab. and associated phenomena". *Progress in Aerospace Science*, **30**, pp. 61–94.
- [7] Durst, and Zanoun, 2002. "Experimental investigation of near-wall effects on hot-wire measurements". *Experiments in Fluids*, **33**, pp. 210–218. 10.1007/s00348-002-0472-1.
- [8] Gaster, M., 1967. The structure and behaviour of laminar separation bubbles. Tech. rep., ARC R&M 3595.
- [9] Gostelow, J. P., and Thomas, R. L., 2006. "Interaction between propagating wakes and flow instabilities in the presence of a laminar separation bubble". No. GT2006-91193, ASME Turbo Expo 2006: Power for Land, Sea and Air, Barcelona, Spain.
- [10] Halstead, D. E., Wisler, D. C., Okiishi, T. H., Walker, G. J., Hodson, H. P., and Shin, H.-W., 1997. "Boundary layer development in axial compressors and turbines: Part 1 of 4—composite picture". *Journal of Turbomachinery*, **119**(1), pp. 114–127.
- [11] Hatman, A., and Wang, T., 1999. "A prediction model for separated-flow transition". *ASME Journal of Turbomachinery*, **121**, pp. 594–602.
- [12] Ho, C., and Huerre, P., 1984. "Perturbed free shear layers". *Annual Review of Fluid Mechanics*, **16**, pp. 365–422.
- [13] Lake, J. P., 1999. "Flow separation prevention on a turbine blade in cascade at low reynolds number". PhD thesis, Air Force Institute of Technology.
- [14] Lin, J., and Pauley, L., 1996. "Low-reynolds-number separation on an airfoil". *AIAA Journal*, **34**, Aug., pp. 1570–1577.
- [15] Lou, W., and Hourmouziadis, J., 1999. "Experimental investigation of periodic-unsteady flat plate boundary layers with pressure gradients". No. FEDSM99-7190, 3rd ASME/JSME Joint Fluids Engineering Division Summer Meeting, San Francisco, CA, USA.
- [16] Lou, W., and Hourmouziadis, J., 2000. "Separation bubbles under steady and periodic-unsteady main flow conditions". No. 2000-GT-0270, 45th ASME International Gas Turbine

- & Aeroengine Technical Congress, Munich, Germany.
- [17] Luo, J., and Lakshminarayana, B., 1997. “Numerical simulation of turbine blade boundary layer and heat transfer and assessment of turbulence models”. *Journal of Turbomachinery*, **119**(4), pp. 794–801.
- [18] Mahallati, A., McAuliffe, B. R., Sjolander, S. A., and Praisner, T. J., 2007. “Aerodynamics of a low-pressure turbine airfoil at low-reynolds numbers: Part 1 — steady flow measurements”. *ASME Conference Proceedings*, **2007**(47934), pp. 1011–1023.
- [19] Mahallati, A., and Sjolander, S. A., 2007. “Aerodynamics of a low-pressure turbine airfoil at low-reynolds numbers: Part 2 — blade-wake interaction”. *ASME Conference Proceedings*, **2007**(47934), pp. 1025–1037.
- [20] Mayle, R., 1991. “The role of laminar-turbulent transition in gas turbine engines”. *ASME Journal of Turbomachinery*, **113**, pp. 509 – 537.
- [21] McAuliffe, B. R., 2006. “Numerical study of instability mechanisms leading to transition in separation bubbles”. No. GT2006-91018, ASME Turbo Expo 2006: Power for Land, Sea and Air, Barcelona, Spain.
- [22] McAuliffe, B. R., and Yaras, M. I., 2005. “Separation-bubble-transition measurements on a low-re airfoil using particle image velocimetry”. *ASME Conference Proceedings*, **2005**, pp. 1029–1038.
- [23] McAuliffe, B. R., and Yaras, M. I., 2007. “Transition mechanisms in separation bubbles under low and elevated freestream turbulence”. No. GT2007-27605, ASME Turbo Expo 2007: Power for Land, Sea and Air, Montreal, QC, Canada.
- [24] Miller, J. A., and Fejer, A. A., 1964. “Transition phenomena in oscillating boundary layer flows”. *Journal of Fluid Mechanics*, **18**, pp. 438 – 449.
- [25] Öztürk, B., and Schobeiri, M. T., 2007. “Effect of turbulence intensity and periodic unsteady wake flow condition on boundary layer development, separation, and reattachment along the suction surface of a low-pressure turbine blade”. *Journal of Fluids Engineering*, **129**(6), pp. 747–763.
- [26] Praisner, T. J., and Clark, J. P., 2007. “Predicting transition in turbomachinery - part I: A review and new model development”. *Journal of Turbomachinery*, **129**(1), pp. 1–13.
- [27] Ripley, M., and Pauley, L., 1993. “The unsteady structure of two-dimensional steady laminar separation”. *Physics of Fluids*, **5**, pp. 3099–3106.
- [28] Roberts, S. K., and Yaras, M. I., 2005. “Boundary-layer transition affected by surface roughness and free-stream turbulence”. *ASME Journal of Fluids Engineering*, **127**, pp. 449 – 457.
- [29] Roberts, W., 1980. “Calculation of laminar separation bubbles and their effect on airfoil performance”. *AIAA Journal*, **18**, pp. 25–31.
- [30] Talan, M., and Hourmouziadis, J., 2002. “Characteristic regimes of transitional separation bubbles in unsteady flow”. *Journal of Flow, Turbulence and Combustion*, **69**, pp. 207 – 227.
- [31] Thwaites, B., 1949. “Approximate calculation of the laminar boundary layer”. *Aero. Quart.*, **1**, p. 245.
- [32] Voke, P., and Yang, Z., 1999. “Large-eddy simulation of separation and transition for turbomachinery flows”. In *Industrial and Environmental Applications of Direct and Large-Eddy Simulation*, Vol. 529 of *Lecture Notes in Physics*. pp. 46–63.
- [33] Volino, R., and Hultgren, L., 2001. “Measurements in separated and transitional boundary layers under low-pressure turbine airfoil conditions”. *ASME Journal of Turbomachinery*, **123**, pp. 189 – 198.
- [34] Volino, R. J., and Bohl, D. G., 2004. “Separated flow transition mechanism and prediction with high and low freestream turbulence under low pressure turbine conditions”. *ASME Conference Proceedings*, **2004**, pp. 45–55.
- [35] Yaras, M. I., 2002. “Measurements of the effects of freestream turbulence on separation-bubble transition”. *ASME Conference Proceedings*, **2002**, pp. 647–660.
- [36] Zhang, X., Hodson, H., and Harvey, N., 2005. “Unsteady boundary layer studies on ultra-high-lift low-pressure turbine blades”. *Proceedings of the Institution of Mechanical Engineers, Part A: Journal of Power and Energy*, **219**, pp. 451–460.